Journal of Wind Engineering & Industrial Aerodynamics 183 (2018) 187–197

Contents lists available at ScienceDirect

Journal of Wind Engineering & Industrial Aerodynamics

journal homepage: www.elsevier.com/locate/jweia

Analysis of climatic factors leading to future summer heatstroke risk changes in Tokyo and Sendai based on dynamical downscaling of pseudo global warming data using WRF

Miguel Yamamoto [a,*], Masataka Kasai [b], Tsubasa Okaze [c], Kazumasa Hanaoka [d], Akashi Mochida [a]

[a] Tohoku University, Sendai, Japan
[b] Shimizu Corporation, Tokyo, Japan
[c] Tokyo Institute of Technology, Yokohama, Japan
[d] Ritsumeikan University, Kyoto, Japan

ARTICLE INFO

Keywords:
Heatstroke risk
Future prediction
Wet-bulb globe temperature
Mesoscale meteorological simulation
Dynamical downscaling
Pseudo global warming data

ABSTRACT

This study aims to clarify the regional characteristics of climate change and its impact on heatstroke risk inside the cities of Tokyo and Sendai, Japan. First, meteorological simulations using the Weather Research and Forecasting model (WRF) were performed. Pseudo global warming data were used as the boundary conditions for WRF simulations for the global-scale current and future climates in the 2000s and 2050s. The increase in wet-bulb globe temperature (WBGT) was larger in Sendai than in Tokyo, and the increase in WBGT in the coastal areas of both cities became larger than that in the inland area. Then, heatstroke risk and incidence rate, which represent the potential risk, were analyzed based on the WBGT distribution. Furthermore, contributions of three types of temperature (wet-bulb, globe, and dry-bulb temperatures) in increasing the WBGT were analyzed in order to clarify the primary meteorological factors for the increase in WBGT in each region. It was found that the wet-bulb temperature is the dominant factor in the increase in WBGT in most regions.

1. Introduction

Urbanization causes temperature increases in urban areas, aggravating the increases caused by climate change. The incidence of heatstroke in Tokyo has been rapidly increasing. During the summer of 2010, Japan experienced a serious heat wave, and the number of heatstroke patients transported by ambulances in Tokyo jumped to about six times that of previous years (National Institute for Environmental Studies, 2012). Since 2010, the number of heatstroke patients has remained elevated. The same trend can also be seen in Sendai, which is located about 300 km north of Tokyo. The Intergovernmental Panel on Climate Change has concluded that continued warming of 0.3–4.8 °C by the end of the 21st century is probable (IPCC, 2013). To mitigate the urban heat island (UHI) effect and adapt to urban warming, various countermeasures have been proposed and assessed (e.g., Takebayashi and Moriyama, 2007; Yumino et al., 2015).

Since urban climate is strongly affected by surrounding climate conditions (e.g., sea breezes), numerical analyses of mesoscale climates are necessary. Mochida et al. (1997) conducted numerical analyses of the mesoscale climate in the Tokyo area. Sato et al. (2008) compared the regional characteristics of the atmospheric heat balance for some regions in the Tokyo metropolitan area, using numerical analyses of the mesoscale climate. Sasaki et al. (2008) compared the influence of regional characteristics on the urban climates of Tokyo, Sendai, and Haramachi, Japan, based on the results of numerical analyses of their mesoscale climates.

Moreover, several previous studies have estimated the risk of heatstroke in summer using wet-bulb globe temperature (WBGT) as a thermal index. Ohashi et al. (2014) showed that the incidence rate of heatstroke increased rapidly when the WBGT exceeded 27–28 °C. They used the simulated daily maximum WBGT as an index for outdoor heat stress and estimated the heatstroke risk for Tokyo, Japan in 2010. Kikumoto et al. (2016) estimated both the current and near-future incidence rates of heatstroke in the Tokyo metropolitan areas and predicted that the incidence rate in August would increase by 63% from the 2000s to the 2030s.

We proposed a prediction method of outdoor heatstroke risk using the

* Corresponding author.
E-mail address: yamamoto@sabine.pln.archi.tohoku.ac.jp (M. Yamamoto).

https://doi.org/10.1016/j.jweia.2018.10.001
Received 30 June 2018; Received in revised form 30 September 2018; Accepted 1 October 2018
Available online 3 November 2018

spatial distribution of the daily maximum WBGT obtained from mesoscale meteorological simulations by the Weather Research and Forecasting model (WRF) and the relationship between the daily maximum WBGT and the daily incidence rate (Kasai et al., 2017). This study aims to clarify the regional characteristics of climate change in each city region and its impact on heatstroke risk, based on the results of future heatstroke risk predictions in Tokyo and Sendai. First, heatstroke risk for Tokyo and Sendai in the 2050s was estimated based on meteorological simulations using the WRF model and the pseudo global warming method (Kimura and Kitoh, 2007). Next, incidence rate, which represents the potential risk evaluated from the heatstroke onset probability per unit time for one person, was analyzed in order to clarify the regional characteristics of increased heatstroke risk due to climate change in each region inside the city. Furthermore, contributions of three types of temperature (wet-bulb, globe, and dry-bulb temperatures) to the increase in WBGT were analyzed, in order to clarify the primary meteorological factors influencing the increase in each region.

2. Method for estimating heatstroke risk

We developed a method to evaluate the heatstroke risk by following the conceptual model in the field of disaster prevention detailed in Kasai et al. (2017). Fig. 1 illustrates the conceptual model for disaster risk evaluation (IPCC, 2014). The risk is greatest for locations where the hazard, vulnerability, and exposure intersect.

In this study, the heatstroke risk was defined as the number of outdoor heatstroke patients transported by ambulances. The three indices of hazard, vulnerability, and exposure were defined as the daily maximum WBGT from WRF simulation; the number of heatstroke patients transported by ambulance in the daytime per 1,000,000 persons as the daily heatstroke incidence rate, which is a function of the daily maximum WBGT; and the daytime population density, respectively.

The outdoor WBGT is calculated with WRF results using Equation (1) as follows:

$$WBGT = 0.7T_w + 0.2T_g + 0.1T_d \quad (1)$$

where T_w is the wet-bulb temperature (°C), T_g is the globe temperature (°C), and T_d is the dry-bulb temperature (°C). Equation (2), which was proposed by Tonouchi and Murayama (2008), was selected to estimate T_g. Equation (2) is an empirical formula analyzed from measurement data recorded at meteorological observatories in Japan:

$$T_g = \begin{cases} T_a + 12.1 + 0.0067S - 2.40v^{\frac{1}{2}} & (S > 400) \\ T_a - 0.3 + 0.0256S - 0.18v^{\frac{1}{2}} & (S \leq 400) \end{cases} \quad (2)$$

Fig. 1. Conceptual model for disaster risk evaluations (IPCC, 2014).

where S is global solar radiation (W/m^2), and v is wind velocity (m/s). The solar radiation at the ground surface and the horizontal wind velocity at 10 m were obtained from WRF simulations and used for S and v, respectively.

To define the vulnerability index, the relationship between the observed daily maximum WBGT and the actual number of heatstroke patients transported by ambulance was analyzed. The daily maximum WBGT for Tokyo and Sendai is calculated using hourly meteorological observational data from the automated meteorological data acquisition systems (AMeDAS) provided by the Japanese Meteorological Agency at each district meteorological observatory. The meteorological observatory in Tokyo is near Tokyo station (Otemachi), and that in Sendai is near Sendai station (Tsutsujigaoka). Previous studies (Ohashi et al., 2014; Kikumoto et al., 2016; Kasai et al., 2017) used the same observational data, and it has been shown that the WBGT at meteorological observatories has a strong correlation with incidence rate. Therefore, we used the meteorological data at the same observatories. The actual number of heatstroke patients was extracted from the emergency transport data provided by the fire departments in Tokyo and Sendai. The time period of the data used in this study is 2010–2011 in Tokyo and 2010–2012 in Sendai. In order to consider seasonal acclimation, the relationship between the daily maximum WBGT and the daily incidence rate was analyzed for every half month, although, in the previous studies (Ohashi et al., 2014; Kikumoto et al., 2016; Kasai et al., 2017), the total number of patients during the summer was used for analysis.

Fig. 2 shows the relationship between the daily maximum WBGT and the daily incidence rate for each period. In both Tokyo and Sendai, the threshold value in which the incidence rate increased rapidly was observed at approximately 28–29 °C. The incidence rate in Sendai during July was higher than that during August due to a lack of seasonal acclimation. However, in Tokyo, seasonal acclimation was not evident in the data. Daytime population density per square kilometer based on the Population Census of 2010 (Ministry of Internal Affairs and Communications, 2012) and the Economic Census of 2009 (Ministry of Internal Affairs and Communications, 2011) (Fig. 3) were used as the exposure index. Finally, the total number of heatstroke patients transported by ambulance was estimated as a risk by multiplying the hazard, vulnerability, and exposure.

3. Calculation conditions of WRF simulations

3.1. Outline of the WRF simulations

WRF simulations were performed to obtain distributions of the daily maximum WBGT as the hazard index. Fig. 4 shows the computational domains in Tokyo and Sendai. We ran each WRF simulations from July 1st to September 1st, with the first two weeks used as spin-up. Other calculation conditions and physical schemes used in this study are summarized in Tables 1 and 2, respectively.

3.2. Urban climate projection in the 2050s using the pseudo global warming method

In order to simulate the future climate, we applied the pseudo global warming method developed by Kimura and Kitoh (2007). The meteorological data under a future climate used as boundary conditions for WRF simulations were provided by the summation of the current weather conditions and global warming components (Iizuka, 2018). For the current climate conditions, the National Centers for Environmental Prediction and the National Center for Atmospheric Research reanalysis products in 2008 were adopted. The global warming components were created by calculating the difference in the monthly climatology between the 20-year average of the 2050s (2040–2059) projection and the 2000s (1990–2009) simulation by the General Circulation Model (GCM). In addition, because dynamical downscaling suffers from large

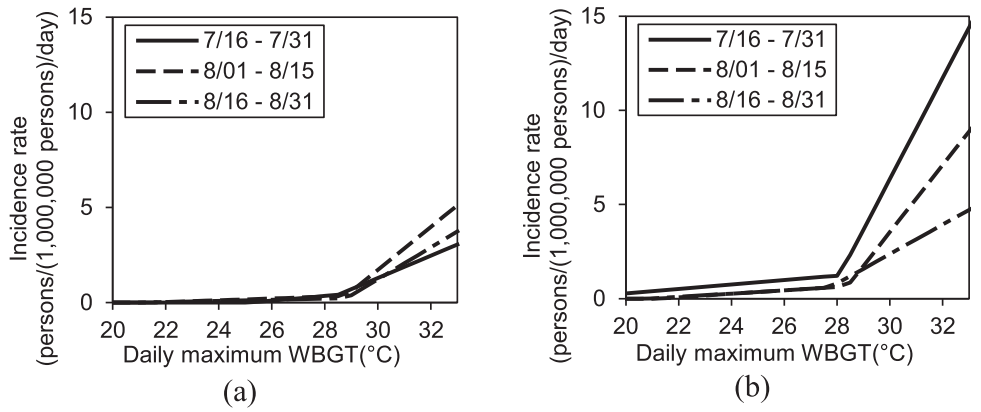

Fig. 2. Relationship between the daily maximum WBGT and the daily incidence rate, (a) Tokyo; (b) Sendai.

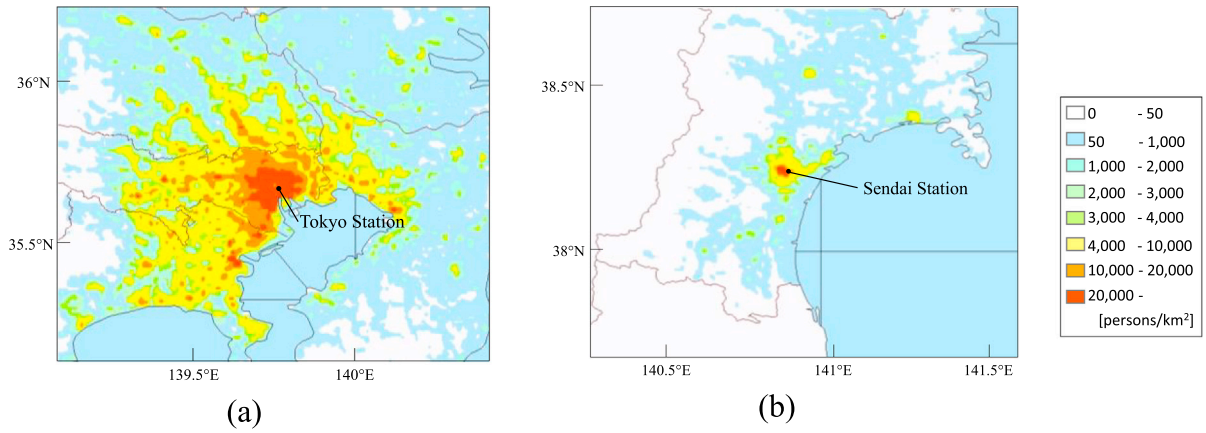

Fig. 3. Daytime population density, (a) Tokyo; (b) Sendai.

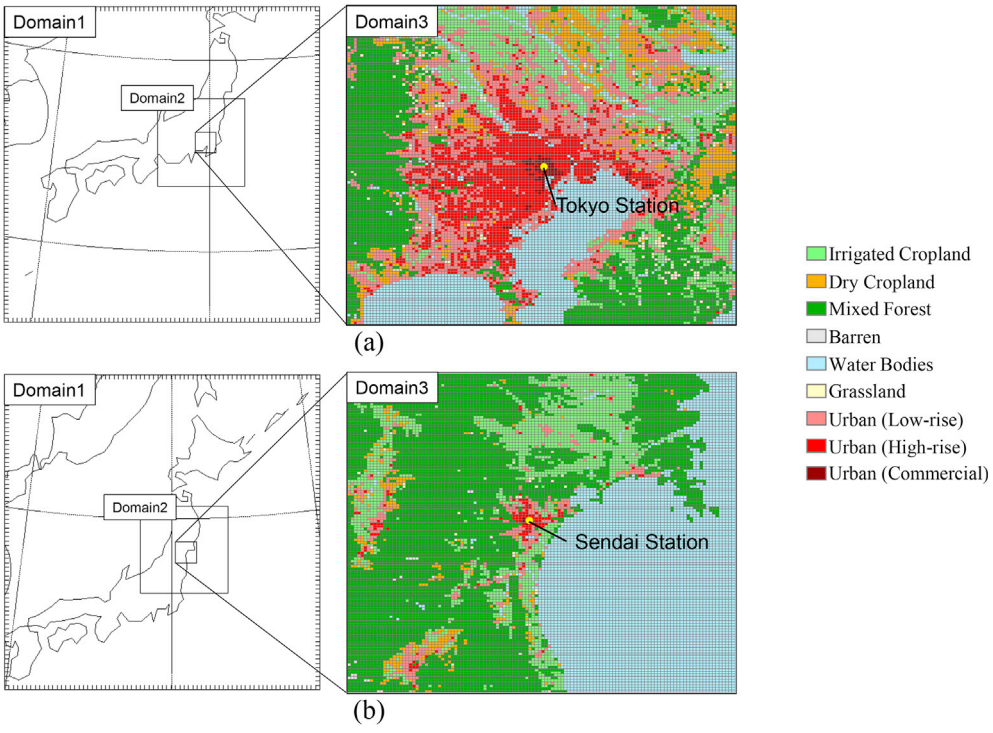

Fig. 4. Calculation domains for WRF simulations and land-use maps for Domain 3, (a) Tokyo; (b) Sendai.

Table 1
Calculation conditions for the WRF simulation.

Items	Content
Date	21:00 (JST) July 1st to 21:00 September 1st
Number of Vertical Grids	34 (from the surface to the 50-hPa level)
Time Interval	Domain 1: 100 s; Domain 2: 20 s; Domain 3: 4 s
Topographic Data	Domains 1 and 2: U.S. Geological Survey Domain 3: Japanese National Land Numerical Information
Nesting	One-way nesting

Table 2
Physical schemes for the WRF simulation.

Items	Content
Microphysics	WRF single-moment six-class scheme (Hong and Lim, 2006)
Shortwave Radiation	Dudhia scheme (Dudhia, 1989)
Longwave Radiation	Rapid radiative transfer model scheme (Mlawer et al., 1997)
Land Surface	Noah land surface model (Chen and Dudhia, 2001) + Single-layer urban canopy model (Kusaka et al., 2001; Kusaka and Kimura, 2004)
Planetary Boundary Layer	Mellor-Yamada-Janjic scheme (Janjic, 2001; Mellor and Yamada, 1982)
Cumulus Parameterization	Domains 1 and 2: Kain-Fritsch (new Eta) scheme (Kain, 2004) Domain 3: None

uncertainties by forcing GCMs, we took an ensemble approach by averaging results from four GCMs (CCSM4, CESM1-CAM5, GFDL-CM3, and INMCM4) to create the global warning data.

4. Results and discussion

4.1. Meteorological factors

Figs. 5 and 6 illustrate the differences between the 2000s and 2050s in air temperature and the absolute humidity at 2-m height, respectively, averaged over the calculation period, July 15th to August 31st. The increases in both air temperature and absolute humidity were larger in Sendai than in Tokyo. In Sendai, the increases in both the air temperature and humidity were particularly high in coastal areas.

Fig. 7 illustrates the differences in sea surface temperature (SST) between the two decades averaged over the calculation period in Domain 1 for the Tokyo calculation. The increase in SST was larger in the northern areas and leads to increases in air temperature and absolute humidity at near-sea-surface levels. The increase in SST was larger in Sendai, which is located 300 km north of Tokyo, which caused the larger increases in air temperature and absolute humidity along its coastal areas, as shown in Figs. 5 and 6.

Fig. 8 shows the distribution of the wind vector averaged over the calculation period in the 2000s. The prevailing wind direction in Tokyo was southerly and that in Sendai was southeasterly. Both directions correspond to the direction of the sea breeze. This advection from the sea transports the air temperature and humidity to the inland area, which induces the large increases in air temperature and humidity along the coastline. The changes in wind vector between the 2000s and 2050s are shown in Fig. 9. The difference in Sendai was small, but the magnitude of the wind in Tokyo became weak in the 2050s. This weak sea breeze in Tokyo leads to less inward transport of humidity in the 2050s, which is one reason that the inland increase in absolute humidity in Sendai was larger than that in Tokyo, as shown in Fig. 6.

The wet-bulb temperature differences between the 2000s and 2050s, averaged over the calculation period of July 15th to August 31st, are illustrated in Fig. 10. The increase in wet-bulb temperature in Sendai was larger than in Tokyo, especially near the coastline in Sendai. This is because the increases in air temperature and absolute humidity were larger in Sendai, but the air temperature in Sendai in the 2050s was still lower than that in Tokyo.

4.2. Daily maximum WBGT

WBGTs were calculated from the results of the WRF simulations. Fig. 11 illustrates the distribution of the daily maximum WBGT averaged over the calculation period, July 15th to August 31st, during the 2050s. In Tokyo, the WBGT was higher than that in Sendai. In both Tokyo and Sendai, the WBGT in inland areas was higher than that in coastal areas. Areas in which the WBGT was particularly low (less than 29.5 °C in Tokyo and 26.5 °C in Sendai) were mountainous areas. Fig. 12 shows the difference between the daily maximum WBGT averaged over one and a half months during the 2050s and 2000s. The WBGT increased in all of the studied areas, with increases in coastal areas being greater than those in inland areas. As discussed in Section 4.1, increases in dry-bulb temperature (i.e., air temperature) and wet-bulb temperature in Sendai, especially in its coastal areas, were larger than those in Tokyo. Subsequently, the increase in WBGT was larger in Sendai than in Tokyo.

4.3. Estimation of incidence rate

The incidence rate is defined as the number of heatstroke patients transported by ambulance in the daytime per 1,000,000 persons. The incidence rate represents the potential risk and is evaluated from the combination of the hazard and the vulnerability. Here, the hazard is defined by the daily maximum WBGT (Fig. 11), and vulnerability is defined as the relationship between the daily maximum WBGT and the

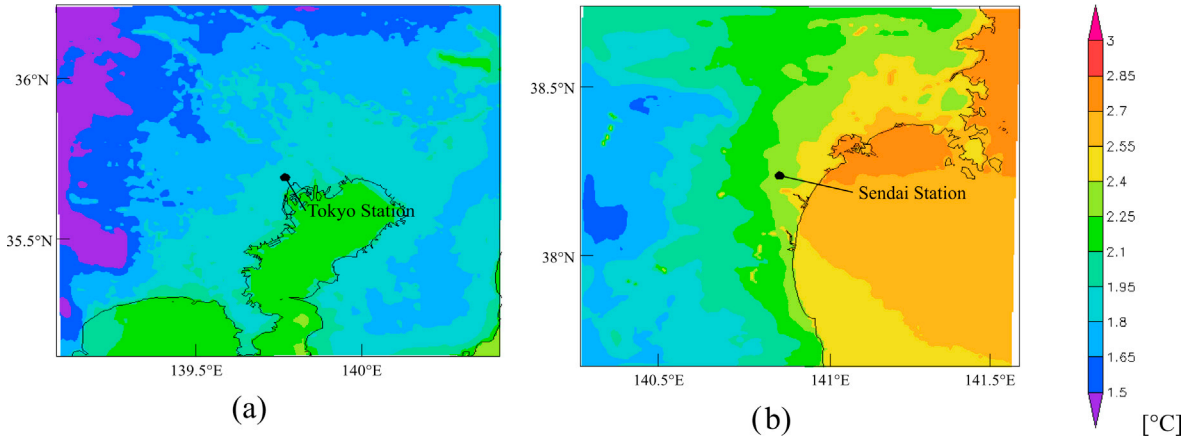

Fig. 5. Differences in mean air temperature at 2-m height from July 15th to August 31st (2050s data minus 2000s data), (a) Tokyo; (b) Sendai.

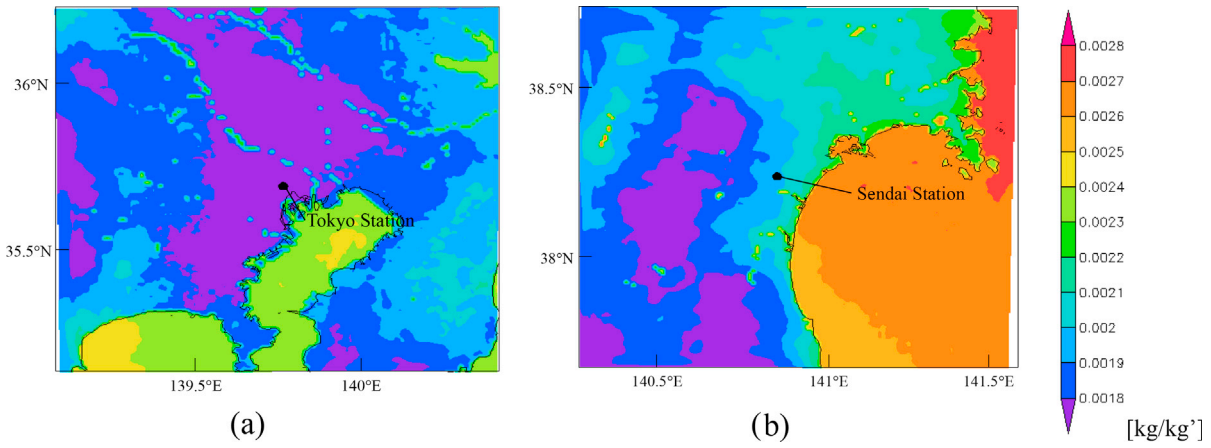

Fig. 6. Differences in mean absolute humidity at 2-m height from July 15th to August 31st (2050s data minus 2000s data), (a) Tokyo; (b) Sendai.

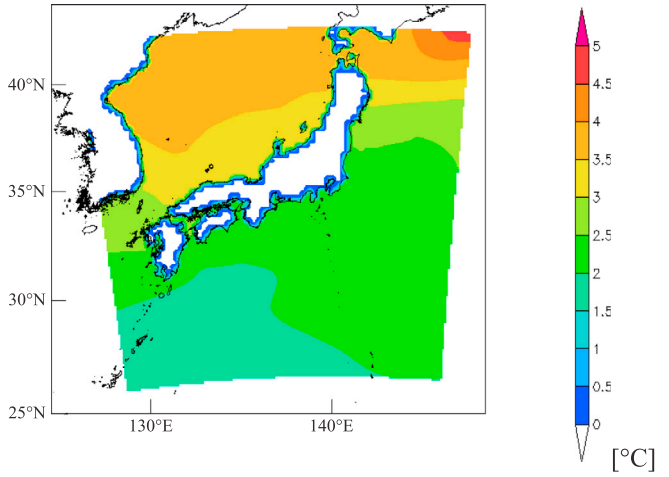

Fig. 7. Differences in mean sea surface temperature from July 15th to August 31st (2050s data minus 2000s data).

number of heatstroke patients transported by ambulance during the daytime (Fig. 2). Therefore, the incidence rate can be estimated from these two factors. Note that the relationship shown in Fig. 2 is only up to 33 °C, although the daily maximum WBGT exceeded 33 °C in a few grids in the 2050s in inland areas. The number of days in which the daily maximum WBGT exceeded 33 °C in at least one mesh was 12 in Tokyo and 1 in Sendai in the 2050s. The maximum value was 34.3 °C. The bias caused by linearly extrapolating the relationship is assumed to be small in this study because the daily maximum WBGT exceeded 33 °C only in small areas inland. Further investigation of the relationship between WBGT values over 33 °C and the incidence rate should be considered for estimating heatstroke risk in more increased global warming cases.

Figs. 13 and 14 illustrate the distribution of the daily incidence rate averaged from July 15th to August 31st during the 2000s and the 2050s, respectively. In both Tokyo and Sendai, the incidence rate was higher in inland areas than in coastal areas due to the relatively high WBGT (Fig. 11).

4.4. Estimation of heatstroke risk

The heatstroke risk is defined as the total number of heatstroke patients transported by ambulance. The heatstroke risk is evaluated from the combination of hazard, vulnerability, and exposure. Here, the incidence rate (Fig. 14) is estimated from the hazard and the vulnerability, and exposure is defined as the daytime population density. Therefore, the heatstroke risk can be estimated from the incidence rate and the exposure.

Fig. 15 illustrates the difference between the daily heatstroke risk averaged over one and a half months during the 2050s and 2000s. Increases in the heatstroke risk value were found to be highest in urban

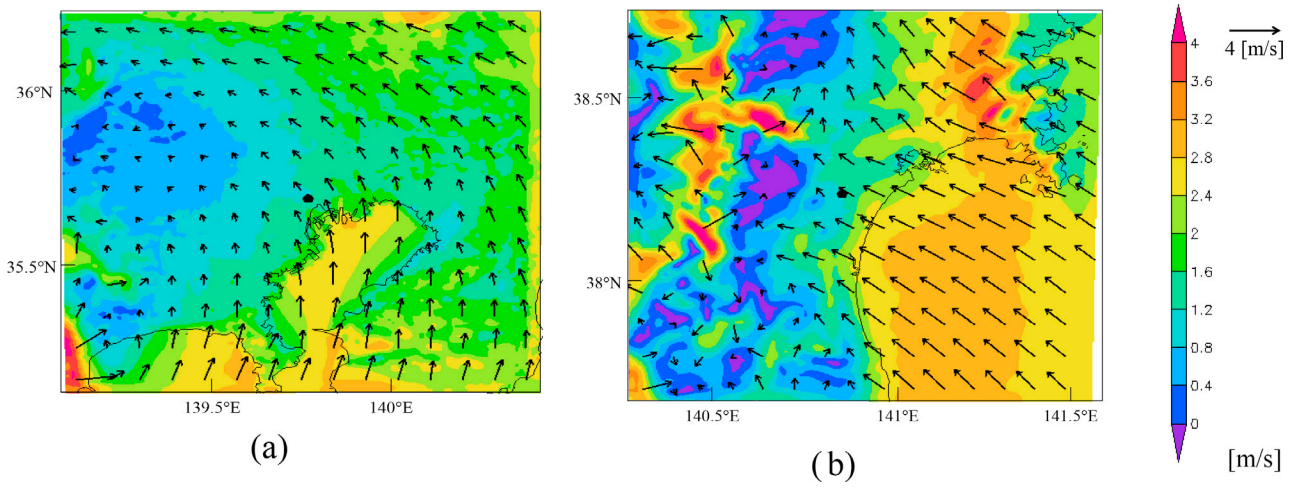

Fig. 8. Mean wind vector at 10-m height from July 15th to August 31st during the 2000s, (a) Tokyo; (b) Sendai.

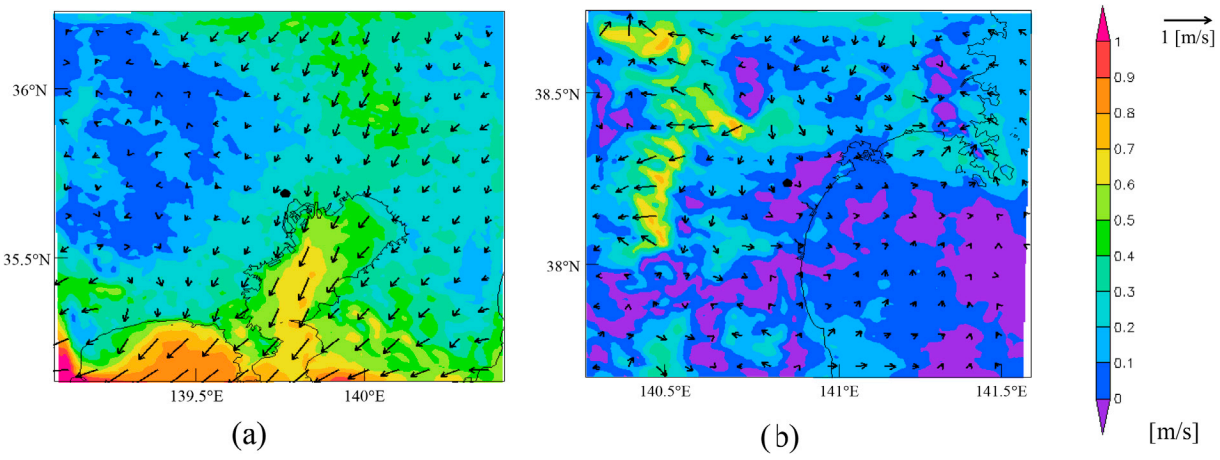

Fig. 9. Differences in the mean wind vector at 10-m height from July 15th to August 31st (2050s data minus 2000s data), (a) Tokyo; (b) Sendai.

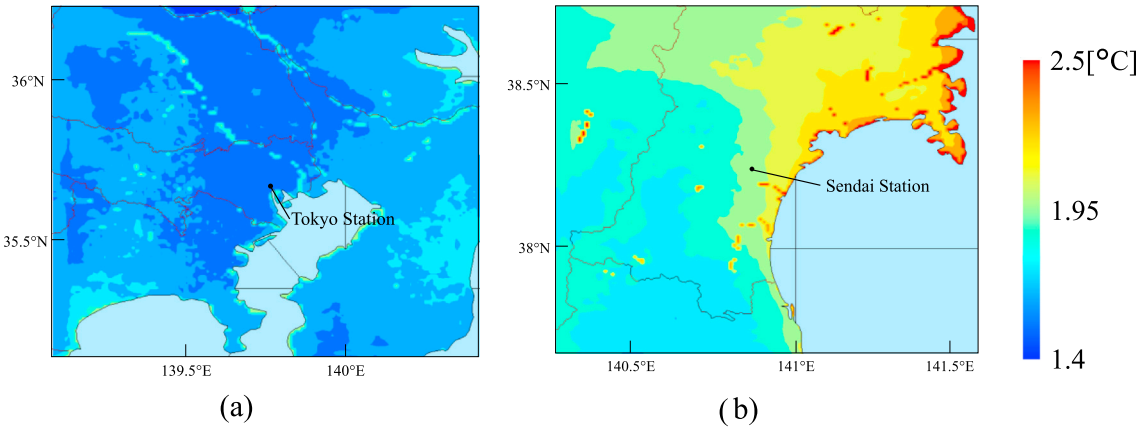

Fig. 10. Differences in the mean wet-bulb temperature from July 15th to August 31st (2050s data minus 2000s data), (a) Tokyo; (b) Sendai.

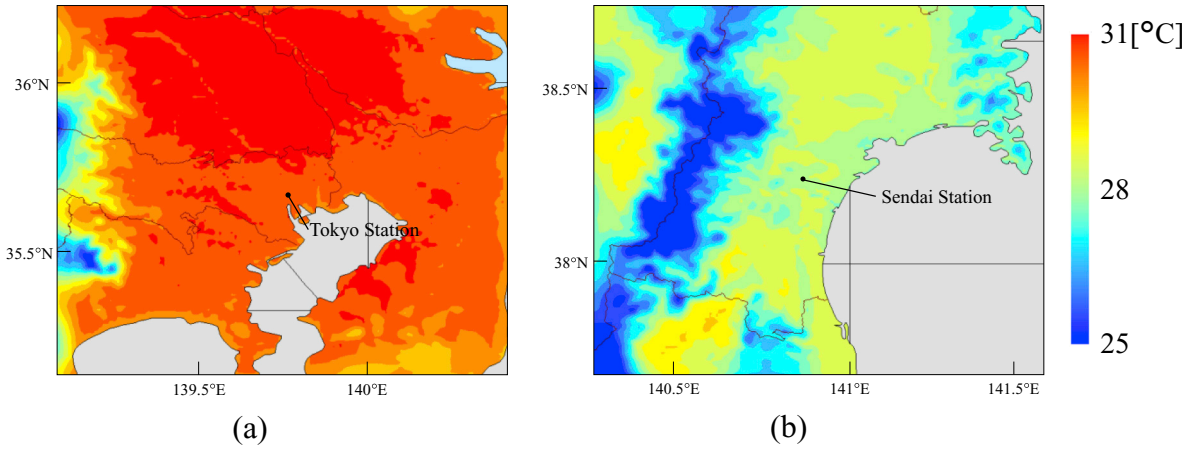

Fig. 11. Mean daily maximum WBGT from July 15th to August 31st during the 2050s, (a) Tokyo; (b) Sendai.

areas. This is because the daytime population density in urban areas (especially in commercial areas) is very high compared with surrounding areas, as shown in Fig. 3. Differences in the heatstroke risk can be calculated by multiplying the daytime population density and the difference in incidence rate. Since the deviation in daytime population density is too large compared with the deviation in the incidence rate difference, the distribution of the heatstroke risk differences is strongly affected by the distribution of the daytime population density.

4.5. *Regional characteristics of heatstroke risk increased by climate change*

The heatstroke risk was greatly affected by population density. The population in Tokyo is approximately ten times that of Sendai. Therefore, the heatstroke risk is not a suitable indicator to investigate the regional

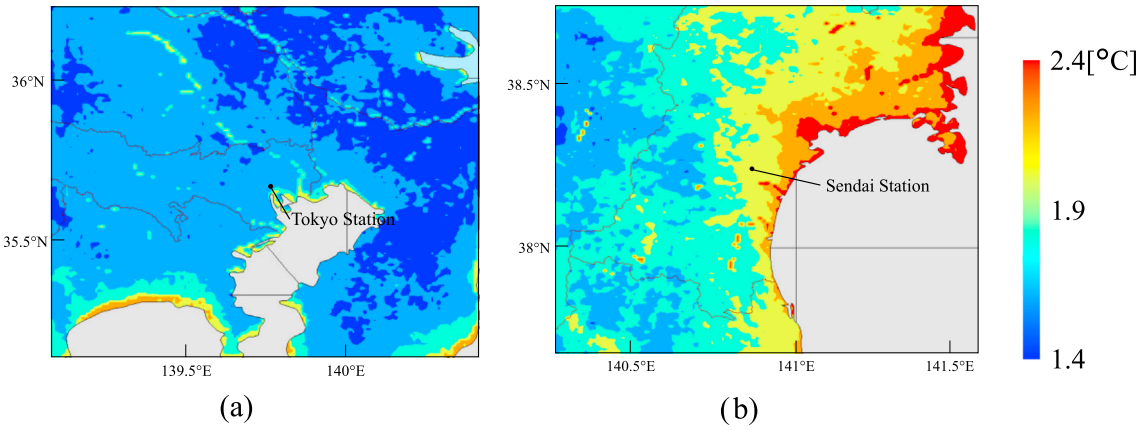

Fig. 12. Differences in the mean daily maximum WBGT from July 15th to August 31st (2050s data minus 2000s data), (a) Tokyo; (b) Sendai.

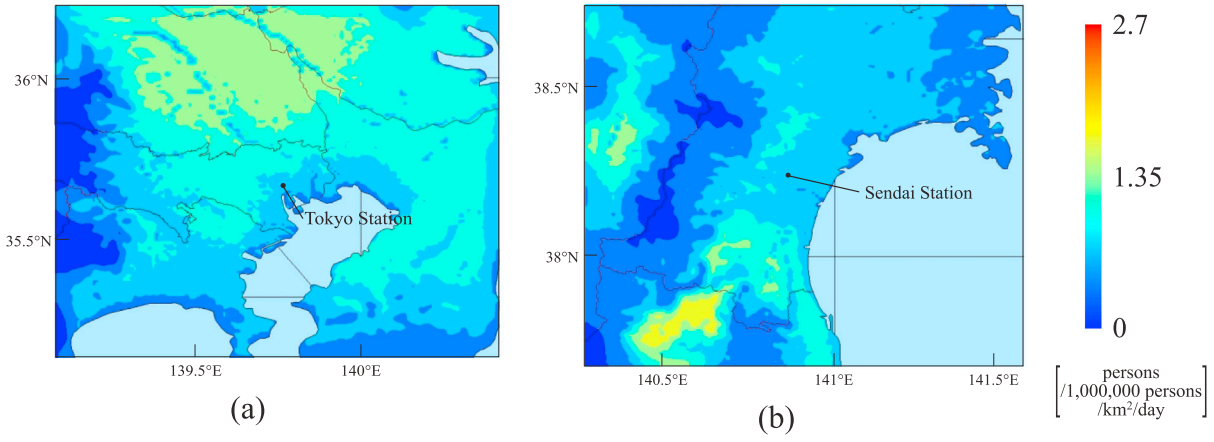

Fig. 13. Mean daily incidence rate from July 15th to August 31st during the 2000s, (a) Tokyo; (b) Sendai.

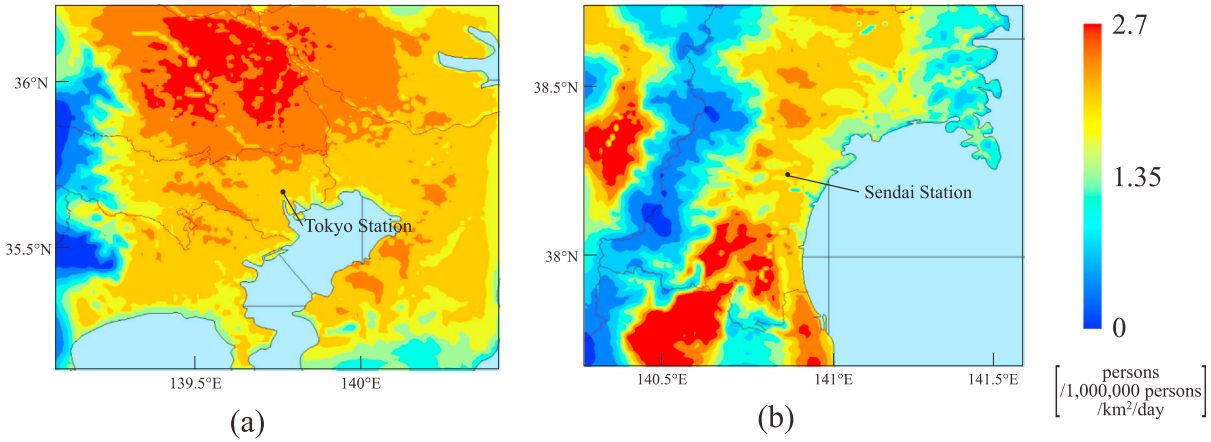

Fig. 14. Mean daily incidence rate from July 15th to August 31st during the 2050s, (a) Tokyo; (b) Sendai.

characteristics of climate change and its impact on heatstroke risk. Therefore, we compared the incidence rate, which represents the potential risk.

Fig. 16 illustrates the difference between the daily averaged incidence rate averaged from July 15th to August 31st during the 2050s and 2000s. Fig. 17 illustrates the distribution of the number of days in which the daily maximum WBGT is higher than the threshold values of the daily maximum WBGT, at which the incidence rate rapidly increases, as shown in Fig. 2. The threshold values used in this study are summarized in Table 3. Fig. 18 shows the difference between the number of days in which the daily maximum WBGT is higher than the threshold values during the 2050s and 2000s.

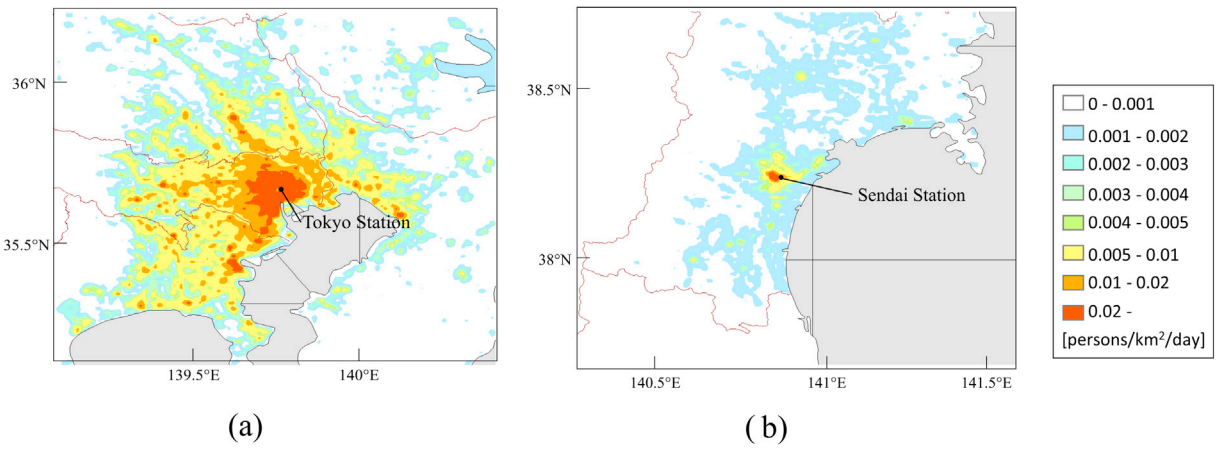

Fig. 15. Differences in the mean daily heatstroke risk from July 15th to August 31st (2050s data minus 2000s data), (a) Tokyo; (b) Sendai.

In Tokyo, the increase in the WBGT value was not large in inland areas; however, there was no significant difference between the inland areas and coastal areas in the increase in the incidence rate value. This is because, in the inland areas, the number of days in which the daily maximum WBGT is higher than the threshold values was already large during the 2000s (Fig. 17). When the daily maximum WBGT is higher than the threshold values, the increase in the WBGT results in a large increase in the incidence rate, as shown in Fig. 2. Therefore, an increase in the WBGT value in inland areas, where the number of days in which the daily maximum WBGT is higher than the threshold values was large during the 2000s, led to a large increase in the incidence rate. In other words, the urban heat inland, which was already severe during the 2000s, becomes much more severe during the 2050s. In addition, in coastal areas of Tokyo, the number of days in which the daily maximum WBGT is higher than the threshold values increased significantly during the 2050s (Fig. 18). In coastal areas of Tokyo during the 2000s, the number of days in which the daily maximum WBGT is higher than the threshold values was small; however, the number of days increased significantly during the 2050s. For this reason, the increase in the incidence rate was large in coastal areas as well as in inland areas. On the other hand, in the coastal areas in Sendai, the number of days in which the daily maximum WBGT is higher than the threshold values was not large during the 2050s; hence, the increase in incidence rate value is small.

In Sendai, the increase in incidence rate in inland areas was greater than that in coastal areas (Fig. 16), although the increase in the WBGT in the inland areas was not greater, as shown in Fig. 12. The increase in the number of days in which the daily maximum WBGT is higher than the threshold values led to the increase in the incidence rate during the 2050s. The number of days in which the daily maximum WBGT is higher than the threshold values was small in coastal areas; therefore, an increase in the WBGT resulted in a smaller increase in the incidence rate than did that in inland areas.

In inland areas of both Tokyo and Sendai, the incidence rate was much higher during the 2050s. In coastal areas of Tokyo, a heatstroke risk that did not exist in the 2000s existed during the 2050s. In coastal areas in Sendai, the incidence rate remained relatively low, even during the 2050s.

4.6. *Meteorological factors contributing to the WBGT increase*

The outdoor WBGT is defined as the summation of wet-bulb temperature (T_w) multiplied by 0.7, globe temperature (T_g) multiplied by 0.2, and dry-bulb temperature (T_d) multiplied by 0.1, as shown in Equation (1). Therefore, the contribution to the increase in WBGT value is defined as shown in Table 4. In order to determine the primary meteorological factors increasing the WBGT in each region, the contribution of the three types of temperature to the increase were analyzed.

Figs. 19–21 illustrate the distribution of the contributions of the three types of temperature to the increase in the WBGT value averaged from July 15th to August 31st. The increase in value was 1–1.5 °C for T_w, 0.1–0.5 °C for T_g, and 0.05–0.15 °C for T_d. The wet-bulb temperature was

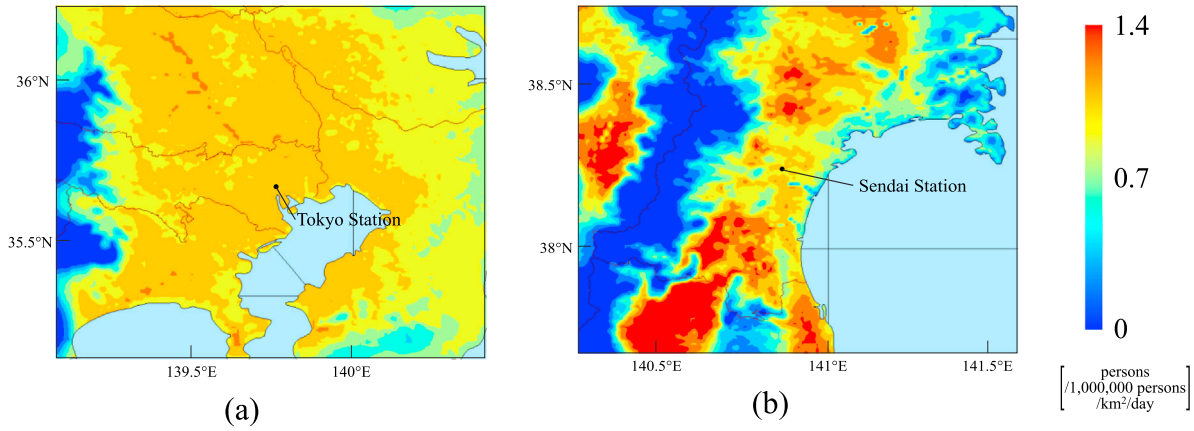

Fig. 16. Differences in the mean incidence rate from July 15th to August 31st (2050s data minus 2000s data), (a) Tokyo; (b) Sendai.

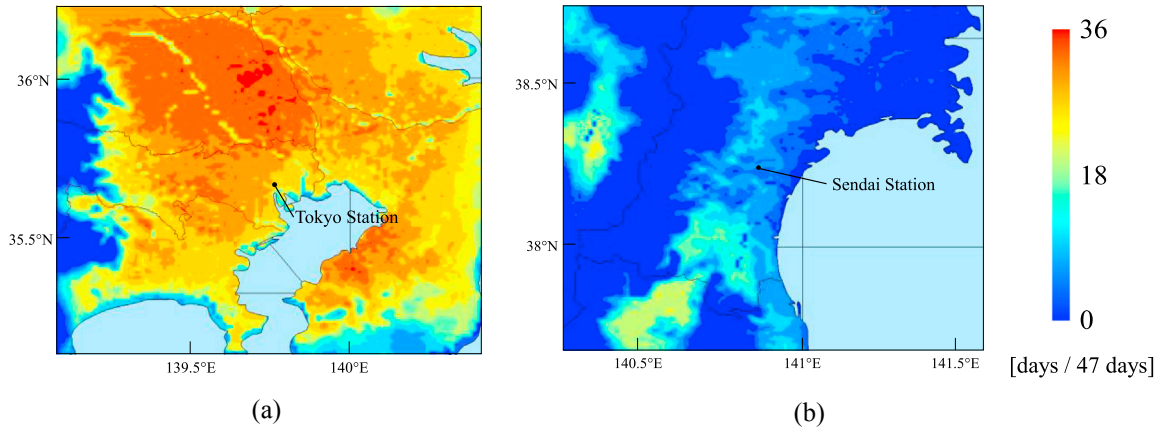

Fig. 17. Number of days in which the daily maximum WBGT is higher than the threshold values from July 15th to August 31st during the 2000s, (a) Tokyo; (b) Sendai.

Table 3
Threshold values [°C].

Period	Tokyo	Sendai
7/16–7/31	28.8	28.1
8/01–8/15	28.8	28.4
8/16–8/31	28.9	27.7

the most influential factor in increasing the WBGT value. Therefore, we can conclude that wet-bulb temperature is the dominant factor increasing the WBGT in most regions. Similar to the increase in WBGT value, the increase in wet-bulb temperature was greater in coastal areas than in inland areas.

5. Conclusions

In this study, the regional characteristics of climate change in each region of Tokyo and Sendai and its impact on heatstroke risk were clarified, based on the results of future heatstroke risk predictions. First, WRF simulations were performed to predict the current and future climates. The pseudo global warming data were used as the boundary conditions for the WRF simulations. Then, the heatstroke risk for Tokyo and Sendai during the 2050s was estimated based on the distribution of WBGT calculated from the results of the WRF simulation. The increase in WBGT was larger in Sendai than in Tokyo, and the increase in WBGT in the coastal areas of both cities became larger than that in the inland areas. This is because the increases in dry-bulb temperature and wet-bulb temperature in Sendai, especially in coastal areas, were larger than those in Tokyo due to the effects of the increase in SST.

Next, incidence rate, which represents the potential risk, was analyzed. In inland areas in both Tokyo and Sendai, the incidence rate was much higher during the 2050s. In coastal areas in Tokyo, heatstroke risk was identified in the 2050s despite its nonexistence in the 2000s. In coastal areas of Sendai, the incidence rate remained relatively low even during the 2050s.

Furthermore, the contributions of the three temperature types (wet-bulb, globe, and dry-bulb) to the increase in WBGT were analyzed, in order to determine the primary meteorological factors affecting the

Table 4
Definition of the contribution to the increase in WBGT value.

Contribution of T_w	$0.7 \times \Delta T_w$
Contribution of T_g	$0.2 \times \Delta T_g$
Contribution of T_d	$0.1 \times \Delta T_d$
ΔT_w, ΔT_g, ΔT_d	Difference in T_w, T_g, T_d(2050s data minus 2000s data)

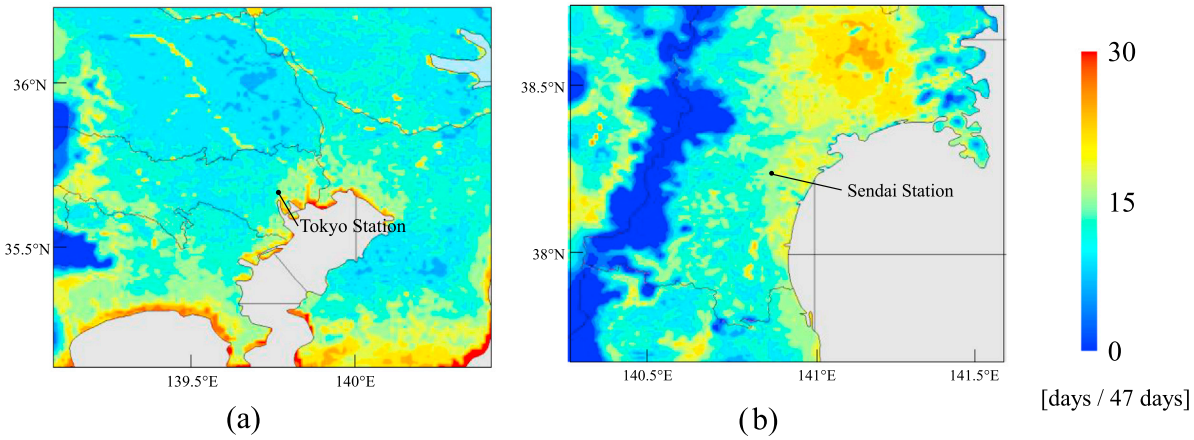

Fig. 18. Differences in the number of days in which the daily maximum WBGT is higher than the threshold values from July 15th to August 31st (2050s data minus 2000s data), (a) Tokyo; (b) Sendai.

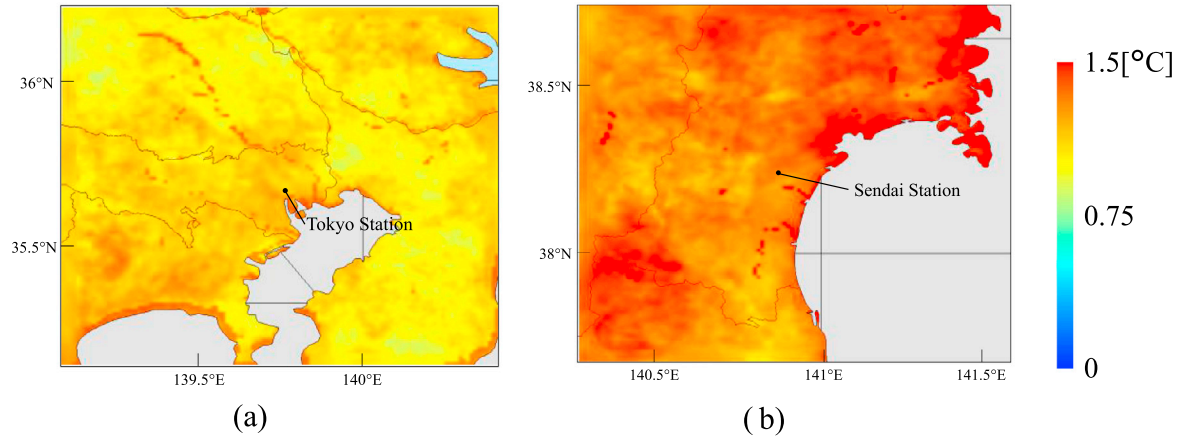

Fig. 19. Mean contribution to the increase in WBGT value of T_w from July 15th to August 31st, (a) Tokyo; (b) Sendai.

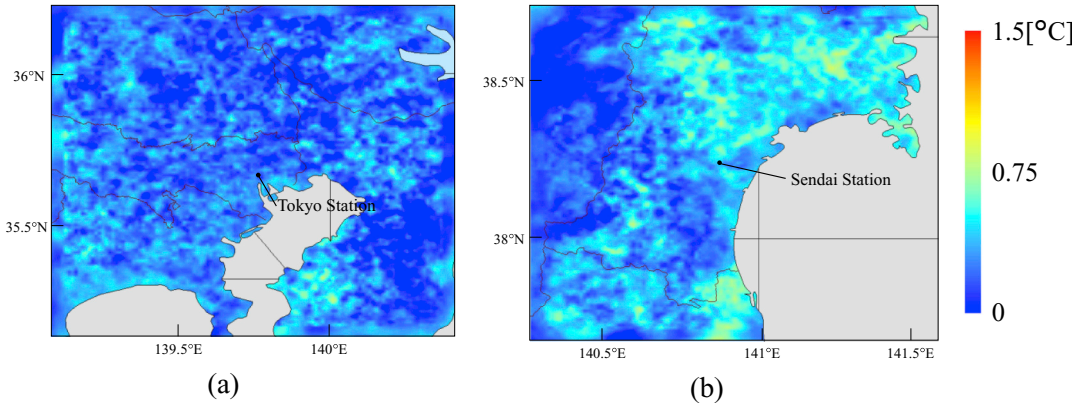

Fig. 20. Mean contribution to the increase in WBGT value of T_g from July 15th to August 31st, (a) Tokyo; (b) Sendai.

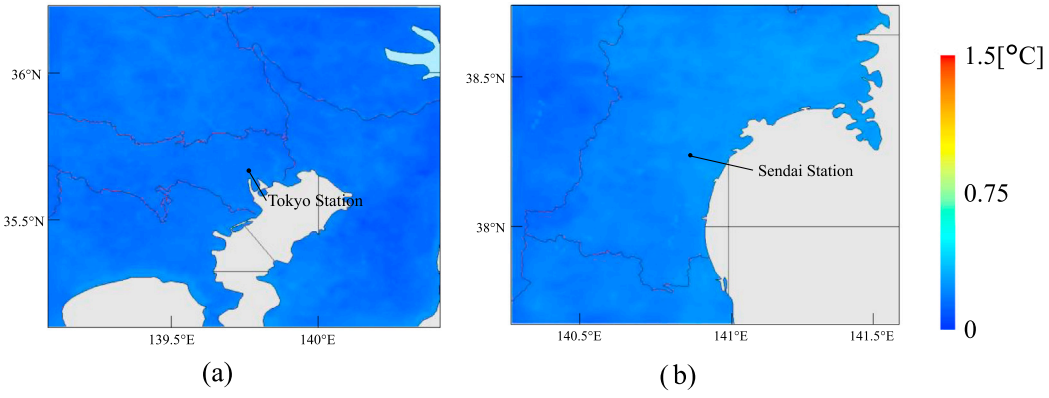

Fig. 21. Mean contribution to the increase in WBGT value of T_d from July 15th to August 31st, (a) Tokyo; (b) Sendai.

increases in each region. As a result, wet-bulb temperature was determined to be the dominant factor increasing WBGT in most regions.

Declarations of interest

None.

Acknowledgments

The authors thank the members of the Working Group for Climate Change Modeling (project general manager: Satoru Iizuka) for providing boundary conditions for WRF. The authors would also like to thank the fire departments of Tokyo and Sendai for providing emergency transport data. This study was supported by the JSPS Grant-in-Aid for Scientific Research (B) [grant number 17H03349] (project general manager: Akashi Mochida) and the joint research project of the Wind Engineering Joint Usage/Research Center at Tokyo Polytechnic University [grant number 172010].

References

Chen, F., Dudhia, J., 2001. Coupling an advanced land surface–hydrology model with the Penn State–NCAR MM5 modeling system. Part I: model implementation and

sensitivity. Mon. Weather Rev. 129, 569–585. <0569:CAALSH>2.0.CO;2. https://doi.org/10.1175/1520-0493(2001)129.
Dudhia, J., 1989. Numerical study of convection observed during the winter monsoon experiment using a mesoscale two-dimensional model. J. Atmos. Sci. 46, 3077–3107. <3077:NSOCOD>2.0.CO;2. https://doi.org/10.1175/1520-0469(1989)046.
Hong, S.Y., Lim, J.O.J., 2006. The WRF single-moment 6-class microphysics scheme (WSM6). J. Kor. Meteorol. Soc. 42, 129–151.
Iizuka, S., 2018. Future environmental assessment and urban planning by downscaling simulations. J. Wind Eng. Ind. Aerod. 181, 69–78. https://doi.org/10.1016/j.jweia.2018.08.015.
Intergovernmentsal Panel on Climate Change, 2013. Contribution of working Group I to the fifth assessment report of the IPCC. In: Climate Change 2013: the Physical Science Basis. Intergovernmental Panel on Climate Change, Geneva, Switzerland.
Intergovernmental Panel on Climate Change, 2014. Contribution of working Group II to the fifth assessment report of the IPCC. In: Climate Change 2014: Impacts, Adaptation, and Vulnerability 2014. Intergovernmental Panel on Climate Change, Geneva, Switzerland.
Janjic, Z.I., 2001. Nonsingular Implementation of the Mellor-yamada Level 2.5 Scheme in the NCEP Meso Model. US Department of Commerce, National Oceanic and Atmospheric Administration, National Weather Service, National Centers for Environmental Prediction.
Kain, J.S., 2004. The Kain–Fritsch convective parameterization: an update. J. Appl. Meteorol. 43, 170–181. <0170:TKCPAU>2.0.CO;2. https://doi.org/10.1175/1520-0450(2004)043.
Kasai, M., Okaze, T., Mochida, A., Hanaoka, K., 2017. Heatstroke risk predictions for current and near-future summers in Sendai, Japan, based on mesoscale WRF simulations. Sustainability 9 (8), 1467. https://doi.org/10.3390/su9081467.
Kikumoto, H., Ooka, R., Arima, Y., 2016. A study of urban thermal environment in Tokyo in summer of the 2030s under influence of global warming. Energy Build. 114, 54–61. https://doi.org/10.1016/j.enbuild.2015.07.033.
Kimura, F., Kitoh, A., 2007. Downscaling by pseudo global warming method. The Final Rep. ICCAP 43–46.
Kusaka, H., Kondo, H., Kikegawa, Y., Kimura, F., 2001. A simple single-layer urban canopy model for atmospheric models: comparison with multi-layer and slab models. Bound.-Layer Meteorol. 101, 329–358. https://doi.org/10.1023/A:1019207923078.
Kusaka, H., Kimura, F., 2004. Coupling a single-layer urban canopy model with a simple atmospheric model: impact on urban heat island simulation for an idealized case. J. Meteorol. Soc. Jpn. 82, 67–80. https://doi.org/10.2151/jmsj.82.67.
Mellor, G.L., Yamada, T., 1982. Development of a turbulence closure model for geophysical fluid problems. Rev. Geophys. 20 (4), 851–875. https://doi.org/epdf/10.1029/RG020i004p00851.
Ministry of Internal Affairs and Communications, 2011. Results of Economic Census, 2009. Available online: http://www.stat.go.jp/data/e-census/2009/index.htm. (Accessed 4 December 2017).
Ministry of Internal Affairs and Communications, 2012. National Census, 2010. Available online: http://www.stat.go.jp/data/kokusei/2010/index.htm. (Accessed 4 December 2017).
Mlawer, E.J., Taubman, S.J., Brown, P.D., Iacono, M.J., Clough, S.A., 1997. Radiative transfer for inhomogeneous atmospheres: RRTM, a validated correlated-k model for the longwave. J. Geophys. Res. Atmos. 102, 16663–16682. https://doi.org/10.1029/97JD00237.
Mochida, A., Murakami, S., Ojima, T., Kim, S., Ooka, R., Sugiyama, H., 1997. CFD analysis of mesoscale climate in the Greater Tokyo area. J. Wind Eng. Ind. Aerod. 67, 459–477. https://doi.org/10.1016/S0167-6105(97)00060-3.
National Institute for Environmental Studies, 2012. Bulletin report on Heatstroke Patients. Available online: http://www.nies.go.jp/gaiyo/archiv/risk8/. (Accessed 4 December 2017).
Ohashi, Y., Kikegawa, Y., Ihara, T., Sugiyama, N., 2014. Numerical simulations of outdoor heat stress index and heat disorder risk in the 23 wards of Tokyo. J. Appl. Meteorol. Climatol. 53, 583–597. https://doi.org/10.1175/jamc-d-13-0127.1.
Sasaki, K., Mochida, A., Yoshino, H., Watanabe, H., Yoshida, T., 2008. A new method to select appropriate countermeasures against heat-island effects according to the regional characteristics of heat balance mechanism. J. Wind Eng. Ind. Aerod. 96 (10–11), 1629–1639. https://doi.org/10.1016/j.jweia.2008.02.035.
Sato, T., Murakami, S., Ooka, R., Yoshida, S., 2008. Analysis of regional characteristics of the atmospheric heat balance in the Tokyo metropolitan area in summer. J. Wind Eng. Ind. 96 (10–11), 1640–1654. https://doi.org/10.1016/j.jweia.2008.02.004.
Takebayashi, H., Moriyama, M., 2007. Surface heat budget on green roof and high reflection roof for mitigation of urban heat island. Build. Environ. 42, 2971–2979. https://doi.org/10.1016/j.buildenv.2006.06.017.
Tonouchi, M., Murayama, K., 2008. Regional characteristics for the risk of heatstroke and HWDI. Jpn. J. Biometeor. 45 (3), S62.
Yumino, S., Uchida, T., Sasaki, K., Kobayashi, H., Mochida, A., 2015. Total assessment for various environmentally conscious techniques from three perspectives: mitigation of global warming, mitigation of UHIs, and adaptation to urban warming. Sustain. Cities Soc. 19, 236–249. https://doi.org/10.1016/j.scs.2015.05.010.